ACS APPLIED MATERIALS & INTERFACES

Research Article

www.acsami.org

Agarose Hydrogel Biomimetic Mineralization Model for the Regeneration of Enamel Prismlike Tissue

Ying Cao,[†,‡] May Lei Mei,[†] Quan-Li Li,*[,‡] Edward Chin Man Lo,[†] and Chun Hung Chu*[,†]

[†]Faculty of Dentistry, The University of Hong Kong, Hong Kong, China

[‡]College of Stomatology, Anhui Medical University, Hefei, China

Supporting Information

ABSTRACT: Laboratory studies have demonstrated that enamel-like mineralized tissue can be regenerated and used to repair enamel loss. This has implications for the management of noncarious tooth loss resulting from dental erosion, attrition, and abrasion. In this study, we designed a hydrogel biomimetic mineralization model for the regeneration of enamel-like mineralized tissue with a prismatic structure. The mineralized tissue, which was generated by the model on an etched enamel surface in the presence of 500 ppm fluoride, was analyzed with scanning electron microscopy, X-ray diffraction, Fourier transform infrared spectroscopy, and the nanoindentation hardness test. The generated tissue had enamel prismlike layers containing well-defined hexagonal hydroxyapatite crystals. The modulus of elasticity and the nanohardness of the regenerated enamel prismlike tissue were similar to those of natural enamel. Thus, the regeneration of enamel using this hydrogel biomimetic mineralization model is a promising approach for the management of enamel loss.

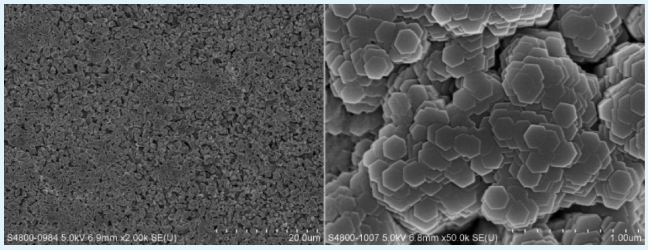

KEYWORDS: *enamel, mineralisation, model, prism, regeneration, nanoindentation*

1. INTRODUCTION

Dental enamel is a highly mineralized tissue made up of approximately 95% substituted hydroxyapatite, 4% water, and 1% organic macromolecules.[1] It consists of nanorod-like hydroxyapatite (HA) crystals arranged into well-organized microarchitectural units called enamel prisms.[2] Enamel prisms are an important factor in the remarkable mechanical properties of dental enamel, which protects teeth from fractures and acid attack.[3] During enamel formation, ameloblasts secrete amelogenin. Amelogenin is approximately 90% organic matrix material. It spontaneously self-assembles into nanospheres that promote the formation and growth of crystallites, which form a well-organized prism pattern.[4] The hydroxyapatite crystals grow rapidly as the enamel matures and the amelogenin degrades into small fractions, resulting in the formation of a highly mineralized tissue with a well-organized microarchitecture. The ameloblasts undergo apoptosis after the enamel is formed. Enamel is a nonliving mineralized tissue that is susceptible to demineralisation by bacterial and chemical acids in unfavorable environments. It is also subject to mechanical damage through attrition or abrasion.[5]

Previous studies have proposed various methods for regenerating the enamel microstructure and repairing enamel defects based on cell-free strategies, including a hydrothermal method using the controlled release of calcium from Ca-EDTA,[3] hydrothermal transformation of octacalcium phosphate rod to HA nanorods in the presence of gelatin,[6] surfactant-supported HA self-assembly,[7] hydrogen peroxide containing calcium phosphate paste,[8] and an electrolytic deposition system at 85 °C.[9] However, all of these methods are performed under conditions of high temperature, high pressure, or extremely low acidity. Recently, amelogenin was used to control enamel remineralisation to form enamel-like HA nanorods under physiological conditions.[10,11] However, amelogenin is difficult to express and purify and is also very expensive, which limits its clinical application.

The initial formation of enamel apatite in nature occurs when a unique gel-like organic matrix interacts with metabolic and intricate cell activities. The enamel at the secretory or matrix formation stage has a gel-like consistency.[12] In that gel-like microenvironment, the mode of crystal growth is different than in aqueous solutions. Busch and co-workers developed a method to mimic the gel-like microenvironment.[13] They used Ca^{2+} and HPO_4^{2-} diffusion in gelatin to induce the formation of enamel-like fluorapatite on human enamel. The physiochemical nature of this gel-like microenvironment more realistically mimics the unique mineralized tissue matrix environment than aqueous solutions.[14] However, gelatin is sol at the physiological temperature, which limits its application. Glycerine was added to increase the melting temperature of gelatin to 40 °C, but this could be a concern for biosafety when applied in an oral environment for a long time. Agarose is a natural polysaccharide with good biocompatibility; it has been widely used in biomedicine. The temperature of the sol–gel

Received: October 11, 2013
Accepted: December 19, 2013
Published: December 19, 2013

transition of agarose is about 60 °C, which can overcome the limitation of gelatin. In this study, we demonstrated that an enamel prismlike structure can be regenerated by an agarose hydrogel biomimetic mineralization model under physiological conditions using agarose without using cell and/or enamel protein.

2. MATERIALS AND METHODS

2.1. Tooth Slices Preparation. This study was approved by The University of Hong Kong/Hospital Authority Hong Kong West Cluster Institutional Review Board (IRB UW10-210). Extracted sound human third molars were collected with patients' consent. The teeth were disinfected with 3% sodium hypochlorite and rinsed with phosphate-buffered saline. Tooth slices of 2 mm in thickness were prepared perpendicular to the longitudinal axis of each tooth using a low-speed diamond saw (IsoMet low-speed saw, Buehler, Lake Bluff, IL, USA). The slices were polished with silicon carbide papers and then ultrasonically cleaned with deionized water. They were stored in a polyethylene tube at 4 °C.

2.2. Hydrogels and Phosphate Solution Preparation. Calcium chloride ($CaCl_2$) hydrogel was prepared by mixing 0.5 g of agarose powder (BioWest regular agarose G-10, Gene Company, Origin, Spain), 1.9 g of $CaCl_2{\cdot}2H_2O$, and 100 mL of deionized water. An ion-free hydrogel was prepared by dissolving 0.5 g of agarose powder in 100 mL of deionized water. Their pH values were adjusted to 6.5 using 0.1 M NaOH and 0.1 M HCl. The mixtures were allowed to swell at 25 °C for 30 min before being heated at 100 °C. The two hydrogels were kept at 60 °C after complete dissolution before use. The 0.26 M phosphate solution (pH adjusted to 6.5) was prepared by dissolving Na_2HPO_4 in deionized water. Sodium fluoride was added to the phosphate solution to obtain a final concentration of 500 ppm fluoride.

2.3. Enamel Regeneration in Hydrogel Biomimetic Mineralization Model. Tooth slices were etched with 37% phosphoric acid for 1 min, rinsed with deionized water, and placed into polyethylene tubes. The slices were first covered with a 2 mm thick layer of $CaCl_2$ hydrogel and then covered with a 2 mm thick layer of ion-free hydrogel. After gelification, the polyethylene tubes were filled with 10 mL of phosphate solution. A four-layer (enamel slice, $CaCl_2$ hydrogel, ion-free hydrogel, and phosphate solution) hydrogel biomimetic mineralization model was then constructed (Figure 1). The polyethylene tubes were sealed and incubated at 37 °C. The phosphate solution was replaced every 24 h, and the hydrogels were replaced every 48 h. Before replacing the hydrogels, the tooth slices were cleaned ultrasonically with deionized water for 20 s. They were taken out for examination after incubation for 2, 4, and 6 days.

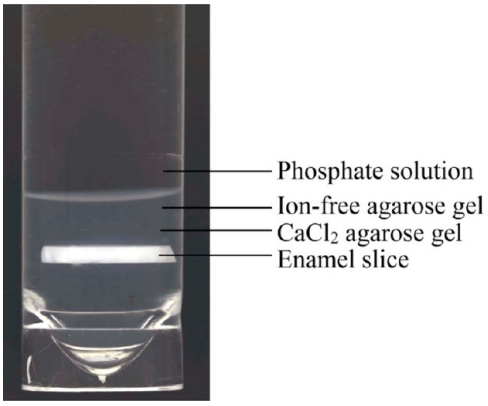

Figure 1. Four-layer hydrogel mineralization model.

2.4. Assessment of Regenerated Enamel and Hydrogels. The morphology of the precipitates were characterized by a field-emission scanning electron microscope (SEM) and an atomic force microscope (AFM). For SEM, the slices were sputter-coated with gold for observation (S4800, Hitachi High Technologies America, Inc., Dallas, TX, USA). AFM was analyzed using a tapping model etched silicon probe (Dimension Edge, Bruker, CA, USA). The phase composition, structure, and orientation of the regenerated tissue were confirmed by X-ray diffraction (XRD) (X'Pert PRO, Philips, Almelo, The Netherlands). Fourier transform infrared (FTIR) spectra of the regenerated tissue were collected by means of a Multiscope FTIR spectrometer (Nicolet 8700, Thermo Scientific Instrument Co., Hudson, NH, USA). The replaced agarose hydrogels were dehydrated with ethanol and then dried in a critical evaporator for SEM and transmission electron microscopy (TEM) evaluation (Tecnai G2 20, FEI Co., Eindhoven, The Netherlands). Selected-area electron diffraction (SAED) was used to identify the mineral structures in the hydrogel.

2.5. Evaluation of Mechanical Properties. The surfaces of the tooth slices were divided into three sections. The first section was covered with acid-resistant and hydrophobic nail varnish (Revlon, NY, USA) (untreated enamel). The nail varnish was used to protect the enamel surface from treatment such as acid etching and subsequent remineralization so that they can be used as a control for comparison. The second section was covered with nail varnish after being etched with 37% phosphoric acid for 1 min (etched enamel). The third section was etched with 37% phosphoric acid for 1 min (this was the area where regenerated mineralized tissue formed after biomimetic mineralization). Three tooth slices were incubated in the hydrogel biomimetic mineralization model for 6 days. They were then immersed in acetone to remove the nail varnish to expose the three areas of untreated enamel, acid-etched enamel, and regeneration enamel. Subsequently, they were cleaned ultrasonically with deionized water for 20 s and stored in deionized water at 23 °C. The mechanical properties, namely, the elastic modulus and nanohardness, of the regenerated mineralized tissue on the third section were compared to the properties of the untreated enamel and etched enamel on the same tooth slice's surface. A nanoindentation test using the Berkovich tip was used to analyze the elastic modulus and nanohardness of each section (G200, Agilent Technologies, CA, USA). The tip was calibrated with a fused-silica sample prior to evaluation.

The nanoindentation test consisted of three segments: the loading segment, the peak-load holding segment, and the unloading segment. The times for both loading and unloading were 15 s. The holding time was 10 s. Sixteen indentations were made on each section of three tooth slices. Thus, a total of 144 indentations were performed on nine sections from three tooth slices. The maximum force applied during loading and unloading was 10 gf (0.098 N). The applied load forces and the depth of penetration into the samples during the indentation were continuously monitored by computer. The data were recorded and processed by Testworks 4 software (MTS Systems Corporation, Eden Prairie, MN, USA), which calculated the elastic modulus and nanohardness and presented them as force-displacement curves. The differences in the elastic modulus and nanohardness among the three sections of tooth slices were assessed with a two-way ANOVA. A 5% significance cutoff level was used for the statistical analysis. An optical microscope and SEM were used to examine the residual indent impressions.

3. RESULTS

3.1. Assessment of Regenerated Enamel and Hydrogels. Rodlike crystals were found on the enamel surfaces after 2 days of incubation in the hydrogel biomimetic mineralization model (Figure 2a). The rodlike crystals extended out the enamel prism surface after 2 days of incubation. The *c*-axial orientation of these crystals was perpendicular to the enamel prism (Figure 2b). The newly precipitated rodlike crystals on the surface were not densely packed and were relatively separated. The spaces between the rodlike crystals were filled with hydrogel matrix (Figure 2c). The examination of the slices in cross sections found that the rodlike crystals precipitated from the enamel surface (Figure 2d). Notably, the rodlike crystals were not haphazardly distributed, and their orientation was almost perpendicular to the underlying enamel. These

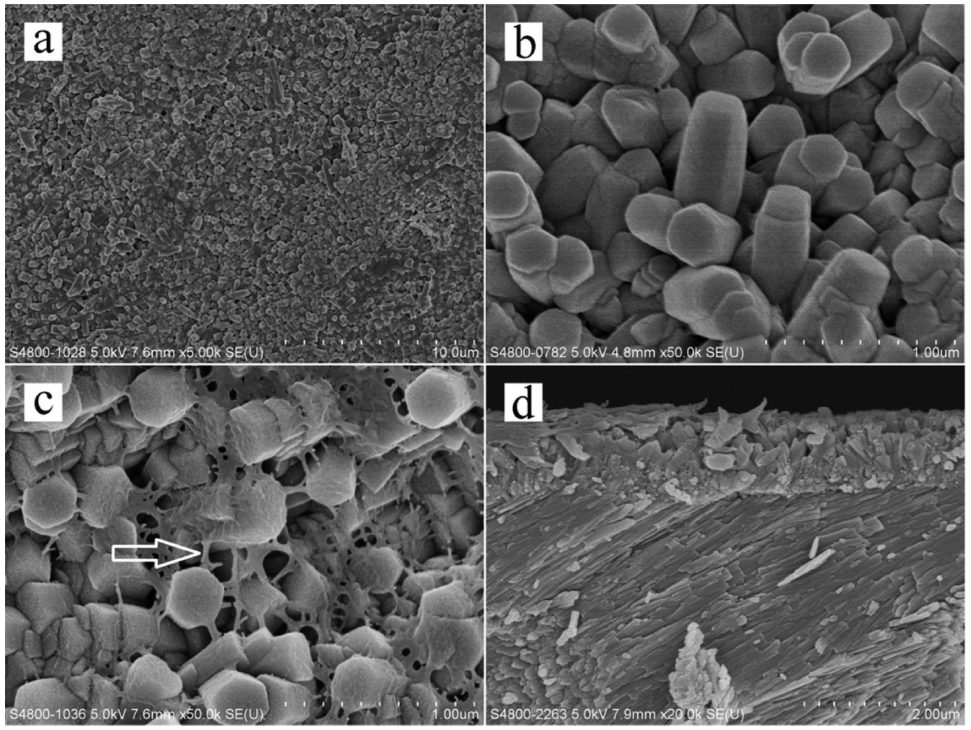

Figure 2. SEM micrographs of the regenerated mineralized tissue after 2 days. (a) Rodlike crystals regenerated on the enamel surface after 2 days. (b) Magnified micrograph of panel a to show that rodlike crystals grew along the *c* axis. (c) Magnified micrograph of panel a to show the crystals and the hydrogel matrix (arrow). (d) Cross-sectional view of the regenerated mineralized tissue to show the crystal orientation and prototype of the enamel prismlike structure.

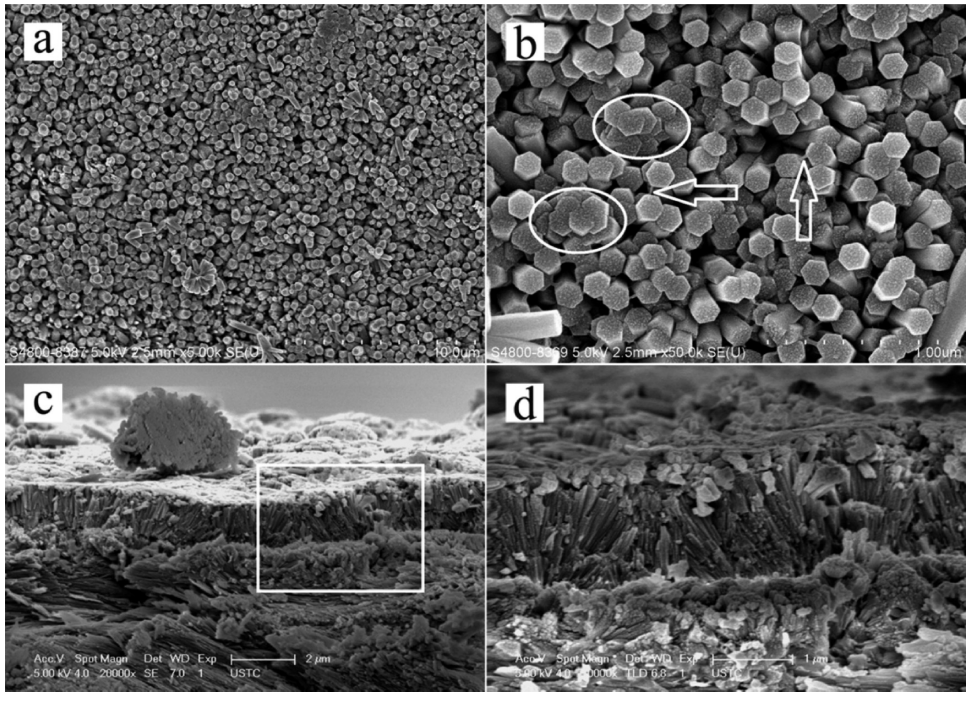

Figure 3. SEM micrographs of the regenerated mineralized tissue after 4 days. (a) Rodlike crystals with a typical apatite hexagonal structure regenerated on the enamel surface. (b) Magnified micrograph of panel a to show the paralleled crystals, the rudiment of the enamel prismlike bundles (oval), and the hydrogel matrix (arrow). (c) Cross-sectional view of panel a. (d) Magnified micrograph of the rectangular area in panel c.

rodlike crystals fused with those in the underlying enamel. The lengths along the *c* axis of the crystals were shorter than that of the growth crystals at 6 days.

Well-defined and orderly distributed rodlike crystals with a typical apatite hexagonal structure were found after 4 days of incubation in the model (Figure 3a). The hexagonal rodlike crystals were approximately 150 nm in diameter and 2 μm in length. They were densely packed along the *c* axis, pushing the rodlike crystals parallel to each other. Certain rodlike crystals self-assemble together to form the rudiment of enamel

dx.doi.org/10.1021/am4044823 | *ACS Appl. Mater. Interfaces* 2014, 6, 410−420

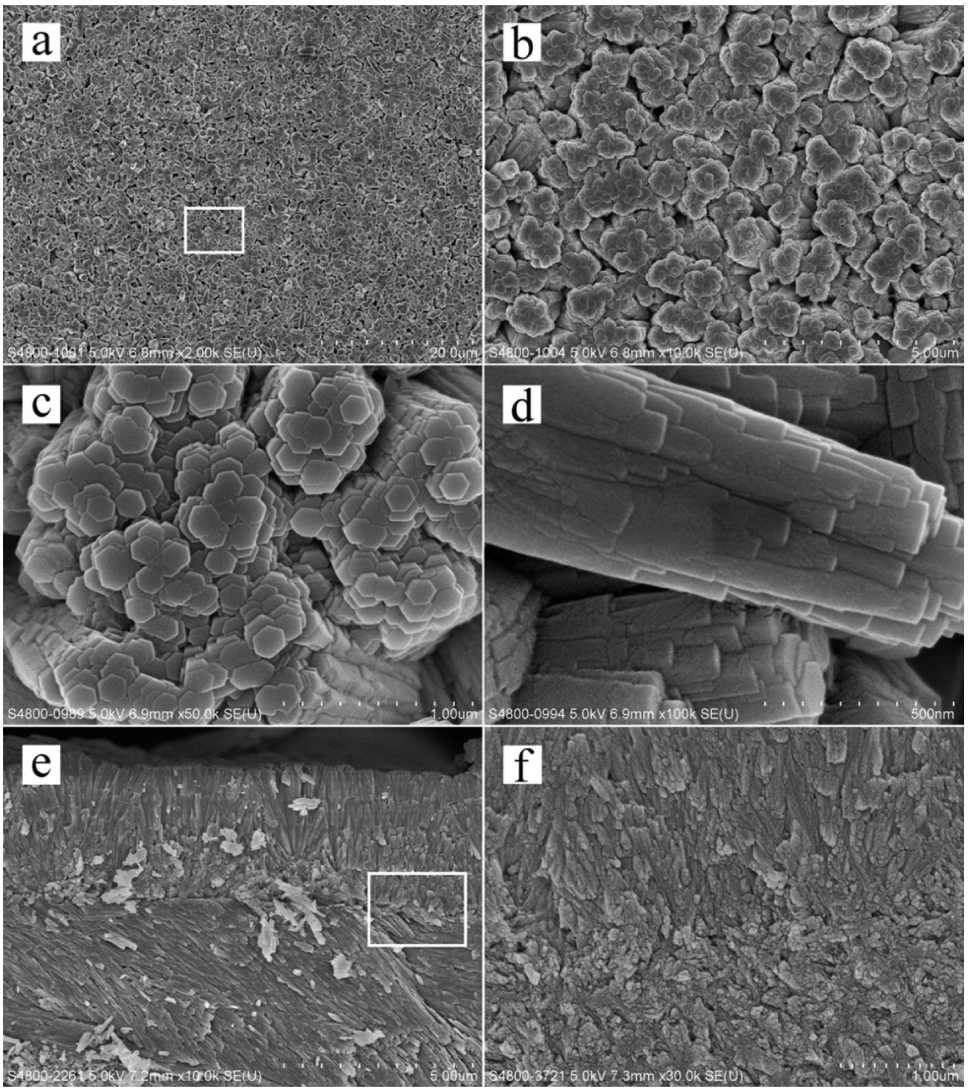

Figure 4. SEM micrographs of the regenerated mineralized tissue after 6 days. (a) Mineralized tissue with enamel prismlike crystals regenerated on the enamel. (b) Magnified micrograph of panel a to show the paralleled bundles. (c) Magnified micrograph of panel a to show the agglomerative hexagonal crystals. (d) Magnified micrograph of the rectangular area in panel a to show the side view of the crystal bundle. (e) Cross-sectional view of panel a to show that the regeneration layer was perpendicular to the underlying enamel. (f) Magnified micrograph of the rectangular area in panel e to show the interface between the regeneration tissue and the underlying enamel.

prismlike bundles (Figure 3b, oval). There was a negligible amount of hydrogel matrix left in the spaces between them (Figure 3b, arrow). The crystallographic *c* axis of these rodlike crystals shared the same orientation, and they were perpendicular to the underlying enamel surface (Figure 3c,d).

The regenerated crystals on the enamel surface formed a homogeneous and dense layer of mineralized tissue after 6 days of incubation (Figure 4a). The strong attraction between adjacent rods caused them to fuse together to form an extensive layer of well-aligned crystals on the enamel surface (Figure 4b). These regenerated crystals had a tendency to spontaneously aggregate, side by side, to form bundles of enamel prismlike structures along the *c*-axis of the rods (Figure 4c,d). The bundled crystals had a width of approximately 1 to 2 μm and were very similar in appearance to the natural enamel surface. These bundled crystals consisted of agglomerative nanocrystals (Figure 4c). They assembled in a well-organized manner and were densely packed to form a homogeneous layer of mineralized tissue on the enamel surface (Figure 4d). Generally, the long axes of the crystals were radially perpendicular to the underlying enamel surface. The thickness of the enamel prismlike surface was approximately 3.5 μm after 6 days (Figure 4e). The interface between the regenerated tissue and the underlying enamel showed a tight agglomeration and fusion (Figure 4f). There was hardly any hydrogel matrix between the crystal bundles.

Figure 5 shows the surface variation in the spatial direction of crystals in 3D AFM images of the acid-etched enamel and the regenerated enamel. The enamel prisms with parallel bundles of hydroxyapatite crystals were observed after the enamel slices were acid-etched for 1 min (Figure 5a). The newly precipitated crystals stuck out from the enamel surface. They were relatively separated and not densely packed on the enamel surfaces after 2 days of incubation in the hydrogel biomimetic mineralization model (Figure 5b). This made the enamel surface rough. The paralleled crystals densely packed along the *c* axis and formed the rudiment of enamel prismlike bundles after 4 days (Figure 5c). The bundles with the enamel prismlike structure were

dx.doi.org/10.1021/am4044823 | *ACS Appl. Mater. Interfaces* 2014, 6, 410−420

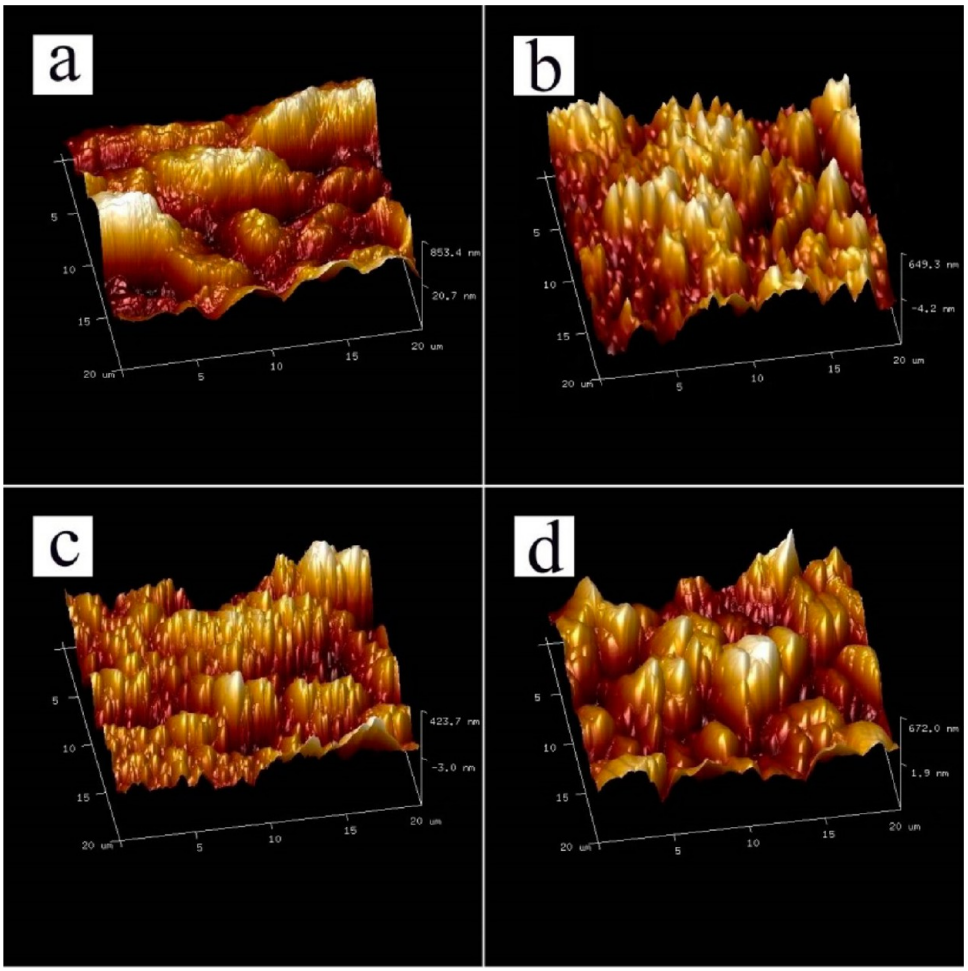

Figure 5. Three-dimensional AFM tapping-mode images of the etched enamel and regenerated mineralized tissue. (a) Etched enamel. (b) Regenerated mineralized tissue after 2 days. (c) Regenerated mineralized tissue after 4 days. (d) Regenerated mineralized tissue after 6 days.

formed after 6 days (Figure 5d), which is similar to sound enamel (Figure 5a). The AFM findings corresponded well to the SEM results.

In this hydrogel biomimetic mineralization model, numerous polymer (agarose fiber)−mineral complex globules were found in the replaced $CaCl_2$ hydrogel adjacent to the enamel surface after 2 days (Figure 6a). These globules were formed by the coalescence of small nanospheres (Figure 6b,c). The blurred ring patterns that formed instead of the sharp and clear arc-shaped patterns in the SAED of the globules suggested an amorphous structure or a very low crystallization (Figure 6d). Very few globules were found in the replaced ion-free hydrogel near the phosphate solution (Figure 6e,f).

The XRD patterns of the regenerated crystals after 2, 4, and 6 days of incubation are shown in Figure 7a. The diffraction peaks (002) at 2θ = 25.8°, (211) at 2θ = 31.8°, (112) at 2θ = 32.2°, and (300) at 2θ = 32.8° corresponded well to the peaks for fluoridated hydroxyapatite (HA) (JCPDS no. 09-0432),[10] suggesting that the crystals were fluoridated HA.[15] The sharp and intense 002 peak indicated that the crystals were well-crystallized and oriented along their *c* axis; these results are consistent with the observations in the SEM images (Figure 5). After 6 days of incubation, the XRD pattern showed that the diffraction peaks around 2θ of 32° were split and clear, which implies good crystallinity of fluoridated HA. Moreover, the (300) diffraction peak was broad, indicating a lattice strain (microstrain) caused by the shift of the nanocrystals from their normal positions. In addition, the peak around 2θ of 44.6° was very sharp, perhaps because of the microstrain caused by the agglomerative individual nanocrystals.[16] These results are consistent with the SEM observation (Figure 4). The FTIR analysis also confirmed the formation of a typical apatite structure over time. The FTIR spectra shown in Figure 7b demonstrate the presence of phosphate groups on the etched enamel surfaces. The splitting PO_4 $\upsilon 4$ band was present in the region of 660 and 520 cm^{-1}. A well-defined and sharp band was observed in the HA. The split PO_4 $\upsilon 3$ band at about 1037 and 1117 cm^{-1} came from HA crystals.[17] There was no −OH group-specific peaks at 1571 cm^{-1}, indicating that the −OH group might be replaced by an F group to form fluoridated HA.[15] It should be noted that some information might be lost because of the reflection mode of FTIR, which makes it difficult to distinguish between FA and HA. Thus, these data should be analyzed in conjunction with other methods, such as XRD and morphological change of the crystals.

3.2. Evaluation of Mechanical Properties. Figure 8 illustrates the typical loading−unloading curves (Figure 8a) and the calculated elastic modulus and nanohardness (Figure 8b) of the untreated, regenerated, and etched enamel. The mean (±SD) elastic modulus and mean nanohardness of the enamel after acid etching were significantly reduced from 90.31 ± 7.63 and 4.28 ± 0.53 GPa (untreated enamel), respectively, to 58.05

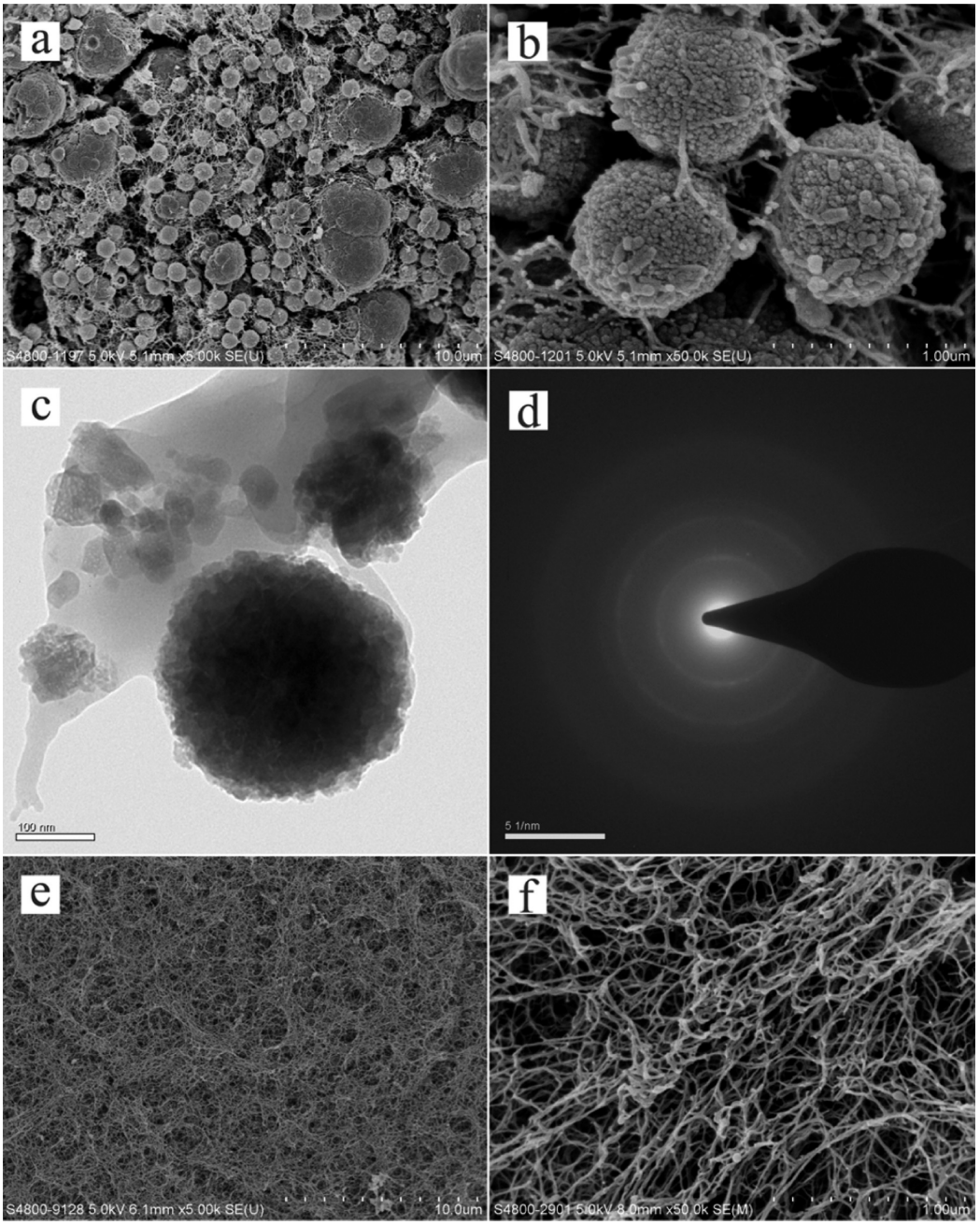

Figure 6. SEM and TEM micrographs of the replaced hydrogel after 2 days. (a) Polymer (agarose fiber)−mineral complex globules in the replaced $CaCl_2$ hydrogel. (b) Magnified micrograph of panel a to show the coalescence of nanospheres. (c) TEM micrograph of the polymer (agarose fiber)−mineral complex globules. (d) SAED pattern of the mineral globule showing no evidence of reflective arcs. (e) A few globules in the replaced ion-free hydrogel. (f) Magnified micrograph of panel e.

± 9.93 and 1.03 ± 0.31 GPa (etched enamel), respectively. After a 6 day incubation, the mean elastic modulus and mean nanohardness of the enamel were significantly increased to 89.46 ± 11.82 and 3.04 ± 0.75 GPa (regenerated enamel), respectively. There were no significant differences in elastic modulus or nanohardness between the regenerated and untreated enamel.

Figure 9a shows an optical microscope image of a regenerated enamel surface with 16 nanoindentations. The nanoindentation impressions form a triangular pyramid. No cracks were found around the indentations. The impression area on the surface of the regenerated enamel (Figure 9c) was similar to that on the untreated enamel (Figure 9b), and both were smaller than on the etched enamel (Figure 9d).

4. DISCUSSION

4.1. Agarose Hydrogel Biomimetic Mineralization Model. The transportation of ions through the organic matrix and the interactions between the ions and the organic matrix are crucial in the regulation of the enamel-mineralization process.[18] The process is mediated by enamel matrix proteins (mainly, amelogenin and enamelin) and can be divided into several phases.[18] The proposed molecular mechanisms for the functions of enamel matrix proteins in enamel mineralization include (i) the prevention of the crystal fusion of premature

dx.doi.org/10.1021/am4044823 | ACS Appl. Mater. Interfaces 2014, 6, 410−420

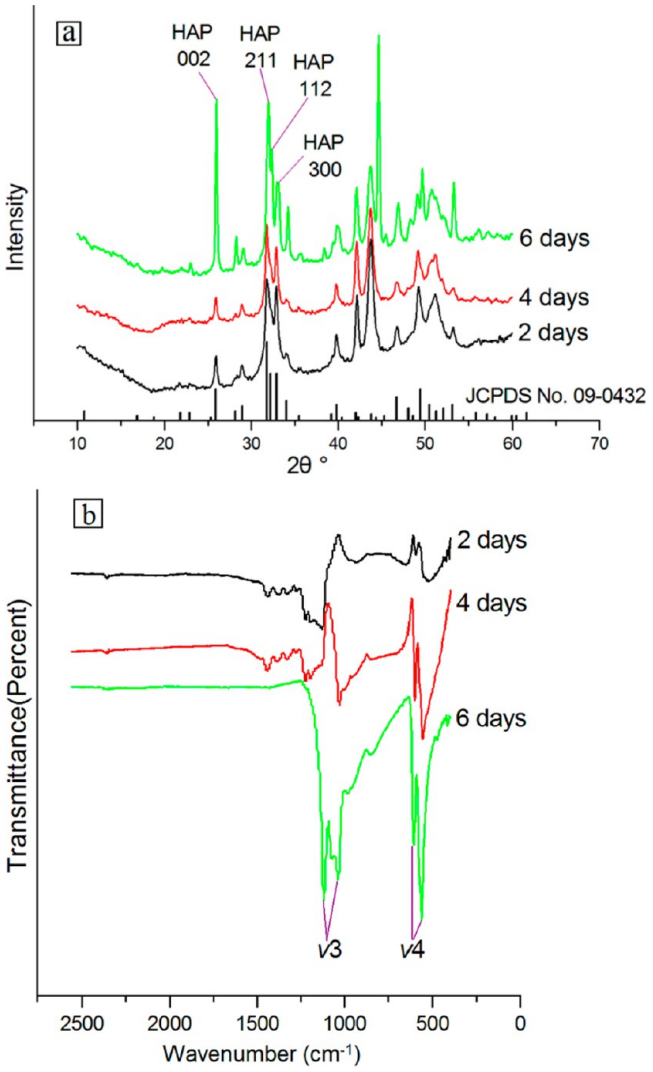

Figure 7. XRD (a) and FTIR (b) spectra of the regeneration layer on the enamel surface after 2, 4, and 6 days.

crystals,[19] (ii) the control of crystal morphology and subsequent elongation,[20] and (iii) the control of the nucleation and growth of the crystals.[21]

At the secretion stage, the enamel organic matrix has a gel-like consistency, which results in enamel apatite formation taking place under a unique gel-like organic matrix environment rather than in aqueous solutions. The mode of crystal growth in a gel-like microenvironment is different than in aqueous solutions. During enamel formation, Ca^{2+} and PO_4^{3-} ions are transported from the layer of ameloblasts into the enamel matrix, where the mineralization takes place. In the process of enamel-matrix secretion and calcification, ameloblasts withdraw from the mineralizing area. There is a unidirectional supply of Ca^{2+} and PO_4^{3-}, and this unidirectional ion supply is thought to play a key role in enamel crystal growth and orientation.[22]

In the present study, agarose hydrogel was used to mimic the gel-like organic matrix environment to induce enamel-like tissue regeneration. A unidirectional supply of Ca^{2+} and PO_4^{3-} were achieved in this model. We found no precipitates of calcium phosphate in the ion-free hydrogel (Figure 6e,f). This suggested that there was little diffusion of calcium ions from the $CaCl_2$ hydrogel to the ion-free hydrogel. On the contrary, the calcium ions accumulated in the $CaCl_2$ hydrogel layer. Meanwhile, the phosphate ions diffused from the PO_4^{3-} solution through the ion-free hydrogel into the $CaCl_2$ hydrogel and enamel surface. Furthermore, the mineralizing precursor of agarose fiber−mineral complex was formed. The organic matrix can prevent premature crystal−crystal fusion, control the subsequent phase transformations, and control the nucleation and growth of the crystals. In our model, the hydrogel stabilized the mineral precursors and prevented them from transforming into crystal (Figure 6). The mineral precursors in the hydrogel were very small and less readily crystallized. This may have contributed to the strong attractive interaction between the agarose polymer and the inorganic surface, which can in turn arrest nucleation and change the shape and size of the primary clusters. The mechanism of the crystal growth will be discussed below.

Agarose is a natural polysaccharide and consists of a linear polymer with repeating units of D-galactose and 3,6-anhydro L-galactose. It is low-cost and biocompatible and has been widely used in biomedicine. Compared to the glycerine-rich gelatin hydrogel model,[13] the temperature of sol−gel transition of agarose is higher than the physiological temperature at which gelatin melts. The mechanical strength of the agarose is higher than gelatin, is safer than the glycerine-rich gelatin hydrogel, and has no ethical concerns. The strength and consistency of

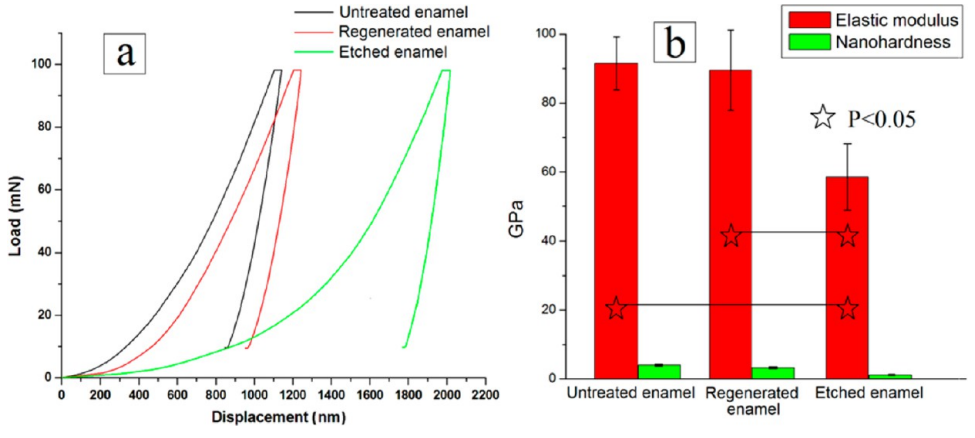

Figure 8. Typical loading−unloading curves (a) and elastic modulus and nanohardness (b) on the untreated, regenerated, and acid-etched enamel after 6 days.

dx.doi.org/10.1021/am4044823 | ACS Appl. Mater. Interfaces 2014, 6, 410−420

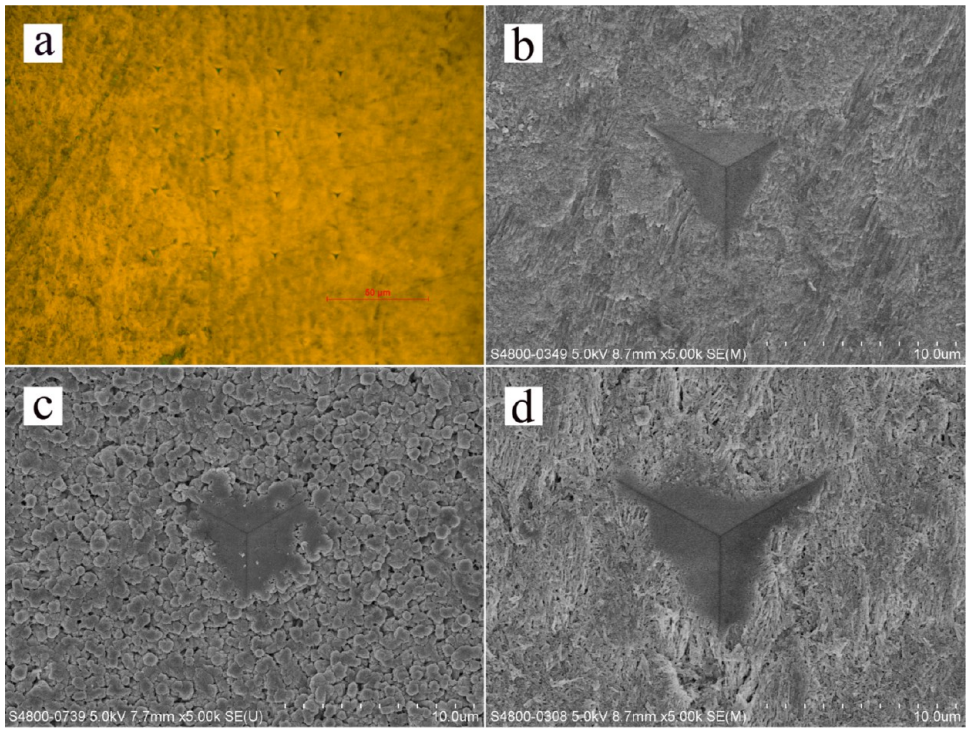

Figure 9. Optical microscope image of the regenerated enamel surface with nanoindentations (a). SEM images of the indentation impression on the surface of untreated enamel (b), regenerated enamel (c), and etched enamel (d).

the hydrogel can be adjusted by varying the concentration and molecular weight of the agarose. These make it easy to transfer to clinical use. However, the mechanism of regeneration of enamel-like tissue is also different between the gelatin model and our agarose model. In the gelatin model, the amino groups of gelatinous polypeptide can form saltlike bonds to phosphate groups on the apatite surface, thus inducing the regeneration of enamel-like minerals.[13] The phosphate groups were entrapped in the gelatin hydrogel, which results as enamel surface-phosphate ions hydrogel. However, in our model, calcium ions were entrapped in the hydrogel, which results in a method with enamel surface-calcium ions hydrogel. If we assembled the hydrogel as enamel surface-phosphate ions hydrogel, then no enamel prismlike tissue could be regenerated in our study. Fan et al. developed an agarose−amelogenin hydrogel model to regenerate the enamel-like tissue.[23] In their model, agarose was used as a releasing agent to investigate the function of amelogenin in the remineralization of early enamel caries. Although the agarose hydrogel containing calcium and phosphate without amelogenin was used as the control group, the different concentration of the inorganic ions and the different diffusion mode gave different results between our study and theirs. Moreover, in the absence of amelogenin, they did not show the regeneration of enamel-like structure. The aim and function of agarose use and the results are different between our study and theirs. Ruan et al. developed an amelogenin-containing chitosan hydrogel for enamel reconstruction through amelogenin supermolecular assembly, stabilizing Ca−P clusters and guiding their arrangement into linear chains.[11] These amelogenin Ca−P composite chains further fused with enamel crystals and eventually evolved into enamel-like crystals anchored to the natural enamel substrate through a cluster growth process. Both the models by Fan et al. and Ruan et al. used amelogenin, but we used an agarose model with no amelogenin to regenerate enamel-like tissue. Our model is simple, low-cost, and biocompatible and can be transferred in a straightforward manner to clinical use, but the mechanism needs further study; it may contribute to its agarose molecules, the concentration of hydrogel, or the concentration of calcium, phosphate, and fluoride.

4.2. Mechanism of Growth of the Enamel Prismlike Crystals. The classical crystallization pathway is a thermodynamic process where ion-mediated crystallization proceeds via a one-step route to the final mineral phase.[24] The nonclassical crystallization pathway is a kinetic process where crystallization proceeds by a sequential process involving structural and compositional modifications of amorphous precursors and crystalline intermediates. Crystallization often involves an initial amorphous phase (such as ACP) that may be nonstoichiometric, hydrated, and susceptible to rapid phase transformation.[25] In biology, a biomineralization process is an organic matrix particle-mediated nonclassical crystallization pathway.[26] The organic matrix controls the mineral crystallites through the molecular interaction between the polymer and minerals with a sequestering mechanism.[27] The amorphous primary particles that are formed by ion or cluster binding at the organic surface can undergo coupled matrix-mediated mesophase transformations, resulting in oriented crystallization with iso-oriented mosaic textures.[24]

Fluoride has an effect on crystal growth during enamel mineralization.[10] In the pilot experiment of this study, well-defined rodlike crystals were formed when 500 ppm fluoride was added into the phosphate solution. Ribbonlike crystals were observed when the fluoride concentration was reduced to 100 ppm, and only platelike crystals were found on the enamel surface in the absence of fluoride. (Figures S1 and S2 in the Supporting Information).

dx.doi.org/10.1021/am4044823 | ACS Appl. Mater. Interfaces 2014, 6, 410−420

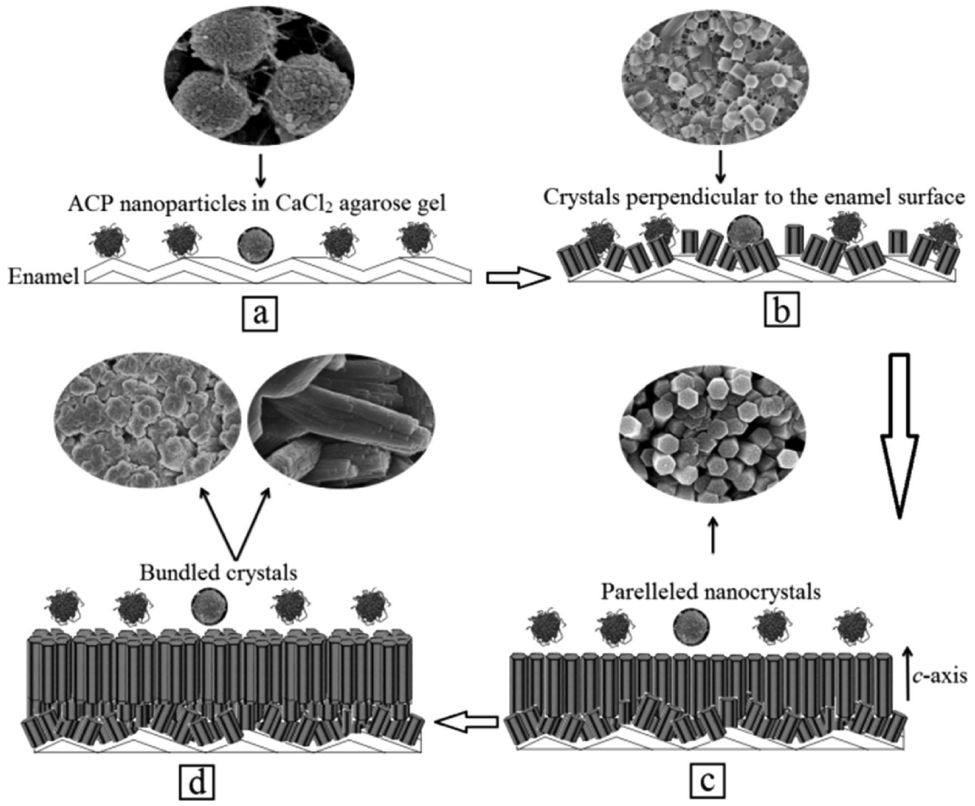

Figure 10. Schematic diagrams demonstrating the nonclassical crystallization pathway. (a) ACP nanoparticles nucleated on the lattice of the enamel HAP crystals. (b) Initial precipitated crystals grew along its *c* axis, which is perpendicular to the enamel prism surface. (c) Well-defined hexagonal crystals were evenly distributed and densely packed on the enamel surface. The mode of crystal growth forced the rodlike crystals to align parallel to each other. (d) Long, large hexagonal crystal acted as a primary crystal in the center of the bundles, and short nanorods fused and aligned parallel to the surface of the primary crystal to form the enamel prismlike structure.

The agarose hydrogel in our model functioned as an organic matrix to control the agarose fiber−nano-ACP complex precursors (Figure 6). There was strong attractive interaction between abundant hydroxyl OH groups of agarose molecules and Ca^{2+}. This interaction could arrest nucleation and also change the shape and size of the primary mineral clusters when phosphate ions diffuse into the $CaCl_2$ agarose hydrogel layer. The ACP nanoparticles coalesced and aggregated, consisting of inorganic cores surrounded by an organic component (Figure 6b). In this way, stabilized nano-ACP or low-crystallization HA with anchored organic ligands was produced in the hydrogel matrix (Figure 6). This corroborated the observation that there was a small mineral complex formed in the layer of the ion-free hydrogel (Figure 6e,f). Furthermore, the agarose hydrogel acted as a reservoir to replenish mineral precursors and as a dynamic interface to transport the mineral precursors to the enamel surface for the mineral mesocrystal transformation (Figure 10a). With the consistent diffusion of PO_4^{3-} and F^- into the hydrogel, the metastable ACP nanoparticles kinetically nucleated on the lattice of the enamel HA crystals. The matrix-mediated crystal growth proceeded by mesophase transformation and aggregation of preformed crystalline building blocks (a mesoscale assembly process, Figure 10b,c), resulting in oriented fluoridated HA crystallization and creating single crystals with iso-oriented mosaic textures (Figures 4d and 10d).

In this study, the regeneration of enamel prismlike tissue was monitored over 6 days of incubation. The mineral precursor nucleated on the enamel surface by heterogeneous nucleation after 2 days. It grew along its *c*-axis extension. The resultant crystals were perpendicular to the enamel prism surface. Because of the different orientations of the enamel prisms and the nucleation sites, the fluoridated HA oriented in a disorderly manner. However, the fluoridated HA crystals were perpendicular to the enamel prism surface where they nucleated. The fluoridated HA crystals were unevenly distributed on the enamel surface. The size of the initial grown crystals in the *c* axis was shorter than the crystals grown after 4 and 6 days of incubation (Figures 3 and 4). Moreover, the nucleation sites were relatively far apart, and the hydrogel matrix was involved in the nucleation sites. This could provide more space for fluoridated HA crystal growth. As a result, the diameter of the crystals after 2 days (Figure 2c) was larger than the crystals after 4 and 6 days (Figures 3 and 4). This finding also corroborated the involvement of agarose hydrogel in controlling the crystal growth. As more nucleation sites were formed during the progress of the crystal growth, the amount of agarose hydrogel was gradually reduced. The agarose hydrogel drew back from the mineralizing areas (Figures 3 and 4). This phenomenon is similar to the natural enamel formation where enamel proteins degrade, resulting in enamel crystals maturing to form prismatic structures. Therefore, the well-defined hexagonal crystals were evenly distributed on the enamel surface after 4 days (Figure 3). The crystals grew along the *c* axis and were densely packed. This mode of crystal growth forced the rodlike crystals to progressively align parallel to each other. The long, large hexagonal crystal probably acted as a primary crystal (seed crystal), enabling the short nanorods to fuse and align parallel to the primary crystal surface and formed

dx.doi.org/10.1021/am4044823 | ACS Appl. Mater. Interfaces 2014, 6, 410−420

crystal bundles. However, the nucleation sites were still relatively apart at 4 days, and most of the crystals were still immature intermediates during the crystal self-assembly or phase transformation. Thus, the morphology of these crystals was different from natural enamel crystal. However, certain rodlike crystals self-assemble together to form the rudiment of enamel prismlike bundles (Figure 3b, oval). With the crystal growth and assembly, the enamel prismlike structure was observed after 6 days (Figure.4). The cross sections of the enamel slices revealed formation of a layer of highly mineralized tissue that was composed of parallel-oriented and densely packed homogeneous crystals. The mechanism of enamel prismlike tissue assembly is shown in Figure 10, which is based on the SEM observations in our study and referred to the mechanism of the nonclassical crystallization pathway.[24]

4.3. Mechanical Properties of the Regeneration Tissue. The nanoindentation test was used to compare the mechanical properties of the regenerated enamel surface with the untreated and etched enamel surfaces. The nanoindentation test is a useful tool for studying mechanical properties on a nanoscale.[28] This depth-sensing technique allows the indentation of minute areas of a few square micrometers so that the elastic modulus and hardness of small volumes of enamel can be measured.[29] The elastic modulus and nanohardness obtained from this test should be reasonably acceptable, as no cracks were found around the indentations. It is important to note that the calculation of elastic modulus is based on the unloading curve. The nanoindentation method is therefore applicable to the study of linear, isotropic materials. Enamel consists of mainly apatite crystals and is an orthotropic material. Therefore, errors could arise if there is a pile-up or sinking-in of the enamel surface on the edges of the indent during the indentation process.

The elastic modulus (90 GPa) and nanohardness of the untreated enamel (4.3 GPa) were comparable to the results reported by Habelitz and co-workers[30] (elastic modulus, 88 GPa; nanohardness, 4.3 GPa). To minimize the variations of elastic modulus and hardness caused by the different orientations of the enamel prism, the mechanical tests were performed on the untreated, regenerated, and etched enamel from the same slices. The elastic modulus (89.5 ± 11.82 GPa) and nanohardness (3.04 ± 0.75 GPa) of the regenerated tissue on the enamel surface after 6 days of incubation were comparable to those of the untreated enamel surface. The mechanical examination demonstrated that the enamel prismlike layer was characterized by similar mechanical properties as the untreated enamel, probably because of their similar microstructures. Similar results were also reported by Busch et al.[13]

Wei used fluorapatite cement pastes to fill enamel defects; however, the setting time is very long, and at the initial setting stage, it is easily washed away by saliva. Furthermore, the fluorapatite crystals in the cement are haphazardly arranged and different from the enamel structure.[15] Many researchers prefer using biomimetic mineralization to regenerate prsimlike enamel tissue. In this study, we demonstrated that enamel prismlike tissue can be regenerated in a hydrogel biomimetic mineralization model. Compared to nonhydrogel solution studies, the physiochemical nature of this enamel-regeneration process vividly mimics the unique mineralized tissue matrix environment.[14] It is noteworthy that this model only mimics the gel-like environment in which the initial formation of enamel apatite occurs. Although it is a simplified model, it provides a basis for future research on enamel regeneration. Further studies should add an organic matrix, such as enamel proteins, to the hydrogel biomimetic mineralization model to mimic the enamel matrix. However, this biomimetic mineralization model can be transferred for future clinical applications such as treatment of erosive wear caused by acidic food and inappropriate brushing habits. The $CaCl_2$ agarose hydrogel, ion-free agarose hydrogel, and phosphate agarose hydrogel can be made commercially. They can be overlapped layer-by-layer to form a sandwich structure inside a tray that the patient can wear overnight. Furthermore, the saliva, containing calcium and phosphate ions, and also F^--containing mouthwash can be used as the supplement for mineral ions for the mineralization.

5. CONCLUSIONS

A hydrogel biomimetic mineralization model was designed to regenerate enamel prismlike tissue. The hydrogel regulated the habit, size, and mineral phase of the growing crystals through cooperative interactions with calcium, phosphate, and fluoride ions. The regenerated apatite crystals were found to be highly oriented along the *c* axis with good crystallinity. The present study provides an important basis for future attempts to develop enamel prismlike material. Hopefully, such material could be used as an alternative treatment in clinical dentistry and other biomedical or industrial applications.

■ ASSOCIATED CONTENT

Ⓢ Supporting Information

Crystals formed in the agarose hydrogel model under different fluoride concentrations. This material is available free of charge via the Internet at http://pubs.acs.org.

■ AUTHOR INFORMATION

Corresponding Authors

*(Q.-L.L.) E-mail: ql-li@126.com; Tel: (+)86-551-65118677; Fax: (+)86-551-65111538.

*(C.H.C.) E-mail: chchu@hku.hk; Tel: (+)852-28590287; Fax: (+)852-28587874.

Notes

The authors declare no competing financial interest.

■ ACKNOWLEDGMENTS

This study was supported by grants from the NSFC/RGC Joint Research Scheme (N_HKU 776/10 and no. 81061160511).

■ REFERENCES

(1) Zhou, Y. Z.; Cao, Y.; Liu, W.; Chu, C. H.; Li, Q. L. *ACS. Appl. Mater. Interfaces.* **2012**, *4*, 6901−6910.

(2) Cao, Y.; Liu, W.; Ning, T.; Mei, M. L.; Li, Q. L.; Lo, E. C.; Chu, C. H. *Clin. Oral Invest.* [Online early access]. DOI: 10.1007/s00784-013-1035-y. Published Online: Aug 4, **2013**.

(3) Chen, H. F.; Tang, Z. Y.; Liu, J.; Sun, K.; Chang, S. R.; Peters, M. C.; Mansfield, J. F.; Czajka-Jakubowska, A.; Clarkson, B. H. *Adv. Mater.* **2006**, *18*, 1846−1851.

(4) Fincham, A. G.; Moradian-Oldak, J.; Simmer, J. P. *J. Struct. Biol.* **1999**, *126*, 270−299.

(5) Selwitz, R. H.; Ismail, A. I.; Pitts, N. B. *Lancet* **2007**, *369*, 51−59.

(6) Zhan, J. H.; Tseng, Y. H.; Chan, J. C. C.; Mou, C. Y. *Adv. Funct. Mater.* **2005**, *15*, 2005−2010.

(7) Fowler, C. E.; Li, M.; Mann, S.; Margolis, H. C. *J. Mater. Chem.* **2005**, *15*, 3317−3325.

(8) Yamagishi, K.; Onuma, K.; Suzuki, T.; Okada, F.; Tagami, J.; Otsuki, M.; Senawangse, P. *Nature* **2005**, *433*, 819.

(9) Ye, W.; Wang, X. X. *Mater. Lett.* **2007**, *61*, 4062−4065.

(10) Fan, Y.; Sun, Z.; Moradian-Oldak, J. *Biomaterials* **2009**, *30*, 478−483.
(11) Ruan, Q.; Zhang, Y.; Yang, X.; Nutt, S.; Moradian-Oldak, J. *Acta Biomater.* **2013**, *9*, 7289−7297.
(12) Satoshi, S.; Shimokawa, H. In *Dental Enamel: Formation to Destruction*; Robinson, C., Kirkham, J., Shore, R., Eds.; CRC Press: Boca Raton, FL, 1995; Chapter 4, p 87.
(13) Busch, S. *Angew. Chem.* **2004**, *43*, 1428−1431.
(14) Silverman, L.; Boskey, A. L. *Calcif. Tissue Int.* **2004**, *75*, 494−501.
(15) Wei, J.; Wang, J. C.; Shan, W. P.; Liu, X. C.; Ma, J.; Liu, C. S.; Fang, J.; Wei, S. C. *J. Mater. Sci.: Mater. Med.* **2011**, *22*, 1607−1614.
(16) Ungar, T. *Scripta. Mater.* **2004**, *51*, 777−781.
(17) Chang, M. C.; Tanaka, J. *Biomaterials* **2002**, *23*, 4811−4818.
(18) Cha, C.; Kim, E. S.; Kim, I. W.; Kong, H. *Biomaterials* **2011**, *32*, 2695−2703.
(19) Moradian-Oldak, J.; Tan, J.; Fincham, A. G. *Biopolymers* **1998**, *46*, 225−238.
(20) Iijima, M.; Moriwaki, Y.; Wen, H. B.; Fincham, A. G.; Moradian-Oldak, J. *J. Dent. Res.* **2002**, *81*, 69−73.
(21) Wen, H. B.; Moradian-Oldak, J.; Fincham, A. G. *J. Dent. Res.* **2000**, *79*, 1902−1906.
(22) Iijima, M.; Moradian-Oldak, J. *Biomaterials* **2005**, *26*, 1595−1603.
(23) Fan, Y. W.; Wen, Z. Z. T.; Liao, S. M.; Lallier, T.; Hagan, J. L.; Twomley, J. T.; Zhang, J. F.; Sun, Z.; Xu, X. M. *J. Bioact. Compat. Polym.* **2012**, *27*, 585−603.
(24) Colfen, H.; Mann, S. *Angew. Chem.* **2003**, *42*, 2350−2365.
(25) Cao, Y.; Mei, M. L.; Xu, J.; Lo, E. C.; Li, Q.; Chu, C. H. *J. Dent.* **2013**, *41*, 818−825.
(26) Ning, T. Y.; Xu, X. H.; Zhu, L. F.; Zhu, X. P.; Chu, C. H.; Liu, L. K.; Li, Q. L. *J. Biomed. Mater. Res., Part B* **2012**, *100B*, 138−144.
(27) Gu, L. S.; Kim, Y. K.; Liu, Y.; Takahashi, K.; Arun, S.; Wimmer, C. E.; Osorio, R.; Ling, J. Q.; Looney, S. W.; Pashley, D. H.; Tay, F. R. *Acta Biomater.* **2011**, *7*, 268−277.
(28) Ge, J.; Cui, F. Z.; Wang, X. M.; Feng, H. L. *Biomaterials* **2005**, *26*, 3333−3339.
(29) Finke, M.; Hughes, J. A.; Parker, D. M.; Jandt, K. D. *Surf. Sci.* **2001**, *491*, 456−467.
(30) Habelitz, S.; Marshall, S. J.; Marshall, G. W., Jr.; Balooch, M. *Arch. Oral Biol.* **2001**, *46*, 173−183.